

# SAR Induced by Low and High Directivity Antenna Apertures at Distances Greater than 25 mm from the Body

Md. Anas B. Mazady<sup>1</sup>, G. Schmid<sup>2</sup>, R. Uberbacher<sup>2</sup>, and M. Ali<sup>1</sup>

<sup>1</sup> Department of Electrical Engineering  
University of South Carolina, Columbia, SC 29208, USA  
anas.eee@gmail.com, alimo@cec.sc.edu

<sup>2</sup> Seibersdorf Labor GmbH  
Seibersdorf, Austria  
Gernot.Schmid@seibersdorf-laboratories.at, Richard.Uberbacher@seibersdorf-laboratories.at

**Abstract** — A comprehensive SAR study of low and high directivity antennas operated at distances greater than 25 mm but less than 200 mm from a large homogeneous elliptical phantom is presented. The study considers antennas, such as dipoles, monopoles, planar inverted-F antennas (PIFAs), IFAs, patches, patch arrays, and dipole arrays. SAR estimation methods for low directivity antennas for both near and far field conditions are proposed and elucidated. For directive antennas and arrays radiating directly towards the phantom interesting phenomena are observed that require more detailed investigation.

**Index Terms** — Antennas, arrays, directive, RF exposure, small antennas, specific absorption rate (SAR).

## I. INTRODUCTION

Electromagnetic exposures from wireless transmitters are regulated by respective regulatory bodies that restrict such exposure both for the general public and occupational professionals. The respective exposure limits (specific absorption rate – SAR) for the general public are identified as 1.6 W/Kg averaged over 1-g of tissue as established by the Federal Communications Commission (FCC) [1], and 2.0 W/Kg averaged over 10-g of tissue as established by the European Committee for Electrotechnical Standardization (CENELEC), which refers to exposure limits recommended in [2]. SAR induced in homogeneous and heterogeneous head and body phantoms has been studied for decades leading to new knowledge and standards set forth by respective standards bodies, such as the IEEE [3-4] and ICNIRP [5]. SAR studies have been conducted considering different types and sizes of antennas, various wireless device models, head models, head shapes, and sizes [6-18]. Traditionally from a compliance point of view, wireless device manufacturers

have to measure SAR except for devices that are inherently compliant because of their very low transmit power; for example 1 mW for the FCC and 20 mW for CENELEC.

Given the presence of myriad wireless devices with variety of output power specifications, device geometry and size variations, and antenna geometry and size variations, it is quite overwhelming to fully grasp and quantify SAR as function of simple metrics, such as operating frequency, power, distance from device, and some simple easy to measure antenna characteristics. A simple method of estimation has two benefits, one, it leads to clear understanding by the antenna designer whether the device is in the ballpark to meet the requirements and whether for low power transmitters the device may be automatically exempt from SAR testing given such tests are costly, man-power intensive, and time consuming. With these outcomes in mind our research groups undertook SAR studies of a variety of antenna sizes and geometries when they were operated next to a flat phantom at distances less than 25 mm. The results of the first phase of our research were published in [19-21]. Subsequently, a more extensive study was undertaken to explore any empirical relationships between antenna performance metrics and SAR [22-25]. Based on that comprehensive study SAR estimation formulas were developed for devices that operate at distances 25 mm or less from the body within the frequency range of 300 MHz to 6 GHz [25]. These formulas can be used to estimate the threshold power levels that satisfy both the 1.6 W/Kg and the 2.0 W/Kg SAR limits. These formulas were developed as function of frequency, antenna to body separation, and *antenna free-space bandwidth (BW)*. Later on the results of this study were adopted into an IEC Standard [26].

The reason for choosing the antenna free-space BW for the rationale lies in the fact that BW is the

reciprocal of antenna quality factor ( $Q$ ), and  $Q$  is expressed as the ratio of the stored and radiated energies of the antenna. Since SAR is strongly dependent on the stored near-fields of wireless device antennas (within 5-25 mm from the user's body), an empirical relationship between SAR or threshold power and BW was possible. As mentioned, the empirical formulas were developed considering SAR data of dipole antennas against a flat phantom.

Although that study covered the frequency range of 300-6000 MHz, the antenna to body distances over which the study focused on was less than 25 mm. Furthermore, the study also did not consider the SAR induced by directive antennas radiating directly towards the body. This led us to carry on a follow on further investigation that addresses these particular issues. Some preliminary results and conclusions of this work were presented earlier [27-28].

In this work we report the simulation and experimental results of SAR induced by a variety of electrically small non-resonant dipoles, resonant dipoles, resonant monopoles, planar inverted-F antennas, inverted-F antennas, microstrip patches, patch arrays and dipole arrays. The goal of this paper is to understand the SAR implications due to small low directivity antennas as well as highly directive antennas radiating directly towards the phantom when the antenna to phantom separation distance is within 40-200 mm. Since the distances are large, we considered to use a large elliptical flat phantom as defined in [29].

The details of the simulation and measurement methods are available in our earlier work [25]. Briefly, all simulations were performed using the Remcom Inc. commercial FDTD code called XFDTD. The XFDTD models containing dipole antennas were earlier validated [21] against the half-wave dipole data presented in IEEE Std. 1528-2003. The Liao absorbing boundary condition (ABC) was used to save simulation time. Before doing so, the Liao ABC usage was verified by comparing with PML (perfectly matched layers) ABC data. For impedance simulations, Gaussian pulses were used with automatic convergence at a threshold of -40 dB, while for SAR simulations, a sinusoidal waveform was used. The mesh size was generally uniform (1 mm), except for planar antennas we used graded mesh having a minimum mesh size of 0.25 mm and a maximum mesh size of 1 mm. All SAR measurements were carried out with the antennas placed next to the elliptical flat phantom ELI4 (Schmid & Partner Engineering AG, Zurich, Switzerland) containing tissue equivalent liquids for the respective frequencies. The dielectric properties of the liquids were measured prior to SAR measurements using a dielectric probe kit in combination with a vector network analyzer. All SAR measurements were conducted using the DASY3 system (Schmid & Partner

Engineering AG, Zurich, Switzerland).

As it will transpire from the results and discussions, the issue of SAR at larger distances are governed by many factors including the location of the body (near-field, far field, aperture size to phantom size comparison, aperture directivity etc.).

The paper is organized as follows. First, the simulation and experimental landscape is defined that includes the frequencies, the distances, and the antennas considered in the study. Second, SAR results of low directivity antennas such as dipoles, monopoles, and PIFAs are described. Third, SAR results of directional patch antennas, patch arrays, and dipole arrays are elucidated. Fourth, a detailed comparison of the SAR data among different antenna classes is provided. And finally, an attempt is taken to suggest SAR estimation algorithms for these large distances followed by suggestion for future research works.

## II. ANTENNA AND PHANTOM MODELS

The antenna types studied and their associated operating frequencies are listed in Table 1. Antenna simulation models as well as experimental prototypes were designed and developed for operation at 900, 1900, 2450, 3700, and 6000 MHz to reflect many commercial wireless applications in those frequency bands. Antennas were oriented and placed next to a large elliptical phantom at distances of 40, 100, and 200 mm for SAR calculation and measurements. Here distance,  $d$ , is defined as the distance from the antenna feed point to the phantom. Although data at other intermediate distances could have added more insight for the sake of saving simulation and measurement time, the above distances were considered.

Table 1: Antenna types studied and their associated frequencies. Distances from phantom were 40, 100, and 200 mm for all antennas

| Antenna Type | Frequency (MHz) |      |      |      |      |
|--------------|-----------------|------|------|------|------|
|              | 900             | 1900 | 2450 | 3700 | 6000 |
| Dipole       | X               | X    | X    | X    | X    |
| Monopole     | X               | X    | X    |      |      |
| PIFA air     | X               | X    |      |      |      |
| PIFA surface |                 |      | X    | X    |      |
| IFA          |                 |      | X    | X    |      |
| DB-PIFA      | X               | X    |      |      |      |
| DB-IFA       |                 |      | X    |      | X    |
| Patch        |                 | X    | X    | X    | X    |
| Patch array  |                 | X    | X    | X    | X    |
| Dipole array |                 |      | X    |      |      |

All low directivity apertures are identified in Table 2, while the directive apertures are defined in Table 3. Among directive antennas, microstrip patch antennas printed on FR substrates and then placed on the edge of

a metal box (10 mm thick) were considered. Patches were designed and built for operation at 1900, 2450, 3700, and 6000 MHz. Similarly, corporate-fed four element microstrip patch array apertures were also designed and built for operation at 1900, 2450, 3700, and 6000 MHz. Collinear arrays of 3, 5, and 7 element dipoles were simulated with and without the presence of reflectors for SAR at 2450 MHz only.

Table 2: Low directivity antenna specifics; e.g., sizes and geometrical properties

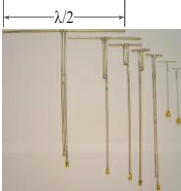
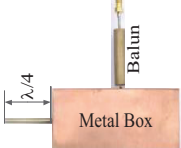

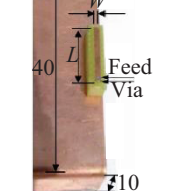
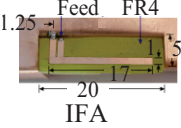
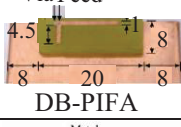
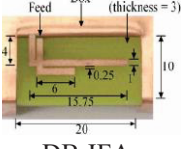
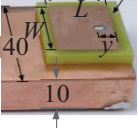
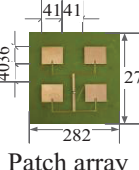
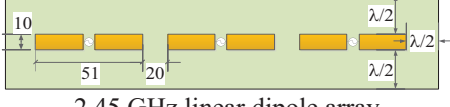
| Photographs   | Description  |
|---|--|
|    | $\lambda/15$ (simulation only) and $\lambda/2$ wire dipoles, center fed; $\lambda/4$ balun used; wire radius=1.8 mm for frequencies up to 2450 MHz and wire radius=0.5 mm at 3700 and 6000 MHz |
| <b>Dipoles</b>  |  |
|    | $\lambda/4$ long, wire radius=1.8 mm; wire on top of a metal box (box dimensions 100 mm by 40 mm by 19 mm)   |
| <b>Monopoles</b>  |  |
|   | $L=40$ mm, $W=31$ mm by 6 mm at 900 MHz and $L=20$ mm, $W=13.5$ mm by 6 mm at 1900 MHz; feed/shorting pin using 1 mm wide strips; spacings of 2.5 and 2 mm at 900 and 1900 MHz                 |
| <b>PIFA air</b>   |  |
|  | $L=16$ mm, $W=1$ mm at 2450 MHz on 100 mm by 40 mm by 10 mm metal box  |
| <b>PIFA surface</b>   |  |
|  | 2450 MHz IFA shown   |
| <b>IFA</b>  |  |
|  | 2450/6000 MHz DB-PIFA  |
| <b>DB-PIFA</b>  |  |
|  | 2450/6000 MHz DB-IFA   |
| <b>DB-IFA</b>   |  |

Table 3: High directivity antenna/array specifics; e.g., sizes and geometrical properties

| Photographs/<br>Diagrams   | Description;<br>Dimensions in mm   |      |      |                |
|--|--|------|------|----------------|
|  | Freq.<br>(GHz)   | $L$  | $W$  | Feed<br>Offset |
|   | 1.9  | 35.5 | 36.5 | 9.25           |
| <b>Patch</b>   | 2.45   | 27.5 | 36.5 | 6.25           |
|  | 3.7  | 17.5 | 24   | 4.00           |
|  | 6.0  | 11   | 15   | 1.00           |
|   | Directivities of 10.9, 13.2, 11.6, and 11.4 dBi at 1900, 2450, 3700, and 6000 MHz respectively. Array approximately 1.5 wavelength. 1.9 GHz array photo shown. |      |      |                |
| <b>Patch array</b>   |  |      |      |                |
|  | 2.45 GHz linear dipole array   |      |      |                |

Dipoles were studied at all frequencies while monopoles were studied at 900, 1900, and 2450 MHz. PIFAs on air or foam were studied at 900 and 1900 MHz to reflect mobile phone frequency bands. Surface mount PIFAs and IFAs were studied at higher frequencies to reflect their operation to support Bluetooth and WLAN type operations. Directional microstrip patches and patch arrays were investigated at 1900, 2450, 3700, and 6000 MHz. All planar antennas were studied both in the conventional (antenna element or array faces away from the body) and flipped orientations (antenna element or array faces the body) with respect to the phantom.

The geometry of the elliptical phantom used is shown in Fig. 1. The phantom consisted of a 2 mm thick shell with dielectric constant  $\epsilon_r=3.7$  and  $\sigma=0$ . The antenna to phantom distance is  $d$ . The tissue dielectric constant and conductivity values are given in Table 4. These values were obtained from [29].

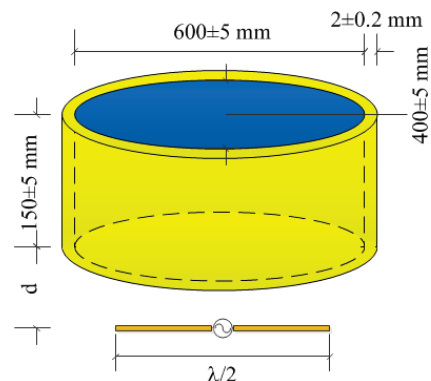


Fig. 1. Geometry of the phantom.

Table 4: Phantom tissue relative permittivity and conductivity. Tissue mass density,  $\rho=1000 \text{ Kg/m}^3$

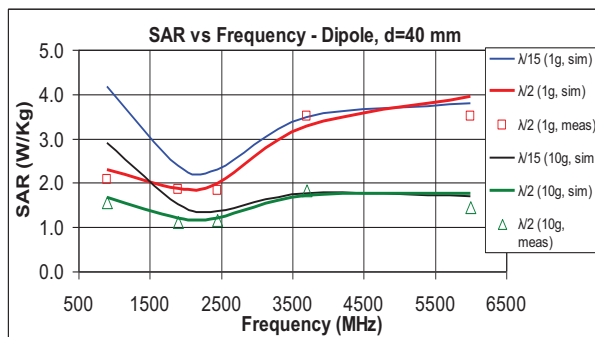
| Frequency (MHz)                     | 900  | 1900 | 2450 | 3700 | 6000 |
|-------------------------------------|------|------|------|------|------|
| Relative Permittivity, $\epsilon_r$ | 41.5 | 40   | 39.2 | 37.7 | 35.1 |
| Conductivity, $\sigma$ (S/m)        | 0.97 | 1.4  | 1.8  | 3.12 | 5.48 |

### III. RESULTS

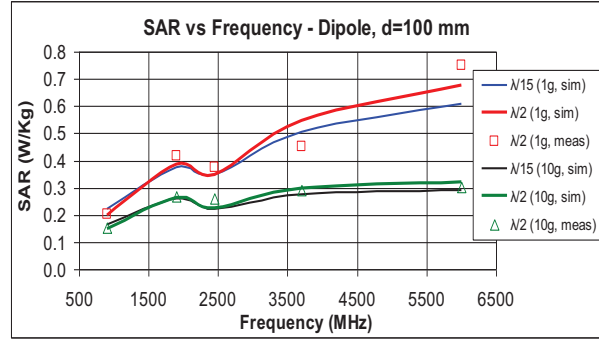
#### A. SAR results of dipole antennas

Computed peak 1-g and 10-g averaged SAR for  $\lambda/15$  and  $\lambda/2$  dipoles placed at  $d=40 \text{ mm}$ ,  $100 \text{ mm}$  and  $200 \text{ mm}$  from the phantom are shown in Figs. 2 (a)-(c). All data are normalized to 1W of power. Measured 1-g and 10-g averaged SAR data for  $\lambda/2$  dipoles are also shown. For all cases, the simulated and measured results are in good agreement. From Fig. 2 (a) for the case when  $d=40 \text{ mm}$ , it is clear that the largest difference in SAR between the  $\lambda/15$  and  $\lambda/2$  dipoles occurs at the lowest frequency (900 MHz). At this frequency the phantom is still in the near field of the antenna. Therefore, the shorter antenna induces almost twice as much SAR than that induced by the longer antenna. As explained in [21], when the phantom is in the near field of the antenna, the shorter antenna acts almost as a point source resulting in a more localized SAR distribution. Also for  $d=40 \text{ mm}$ , as the frequency increases (e.g., at 2450 MHz and higher) the SAR induced by the  $\lambda/15$  and  $\lambda/2$  dipoles are nearly identical to each other as because the aforementioned near field effect disappears.

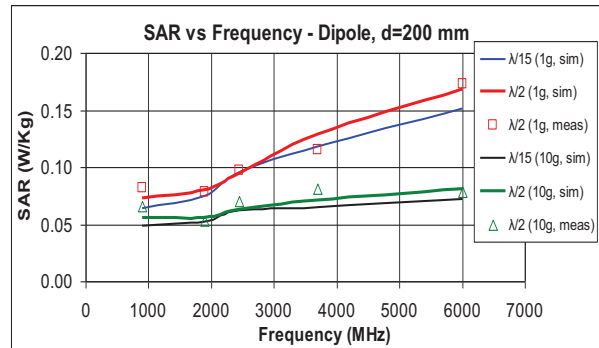
From Figs. 2 (b) and 2 (c) ( $d=100 \text{ mm}$  and  $200 \text{ mm}$ ), it is clear that if the phantom is in the far field of the antennas, the antenna with the slightly higher directivity induces slightly higher SAR. The SAR behavior observed at around 2450 MHz can be explained from the tissue conductivity versus frequency characteristics. The non-linear conductivity increase from 900 MHz to 2450 MHz is responsible for the non-linear SAR profiles shown in Figs. 2 (a) and 2 (c).



(a)



(b)



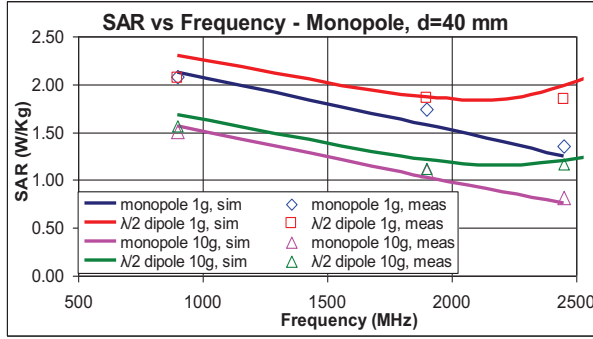
(c)

Fig. 2. SAR versus frequency of dipole antennas for  $d=40 \text{ mm}$ ,  $100$  and  $200 \text{ mm}$ .

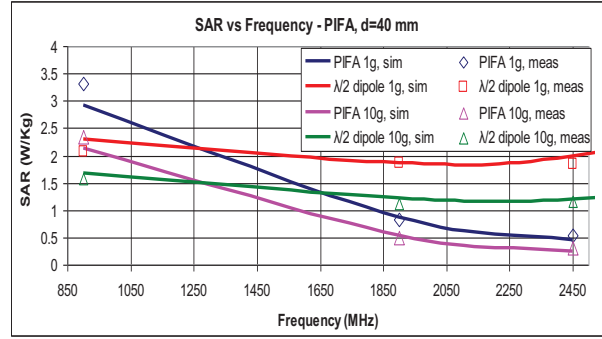
#### B. SAR results of monopole antennas

Computed and measured peak 1-g and 10-g averaged SAR induced by quarter-wavelength long monopole antennas are compared with those induced by half-wave dipoles in Figs. 3 (a)-(c) for  $d=40, 100,$  and  $200 \text{ mm}$ . Note that, since the monopole box measures  $19 \text{ mm}$  in thickness for  $d=40 \text{ mm}$ , the box is at a distance of  $21 \text{ mm}$  from the phantom.

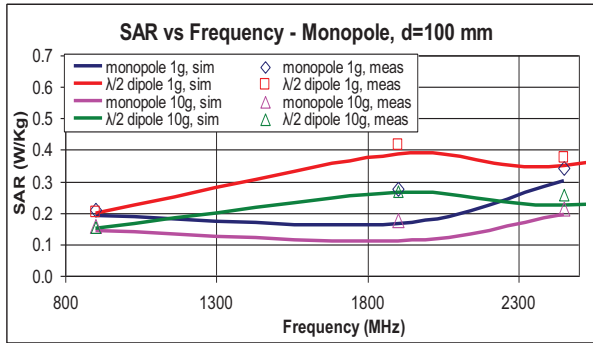
For all three distances, the SAR due to monopole antennas are always smaller than the SAR due to dipole antennas. For  $d=40 \text{ mm}$ , the SAR variation due to monopole antennas with frequency is monotonous (decreases almost linearly with frequency). For  $d=100 \text{ mm}$ , the SAR versus frequency characteristics for the monopoles is similar to that of the dipoles except for the inflection point at  $1900 \text{ MHz}$ . The situation is nearly similar at  $d=200 \text{ mm}$ . At  $100$  and  $200 \text{ mm}$  distances, monopole 1-g and 10-g SAR decrease till  $1900 \text{ MHz}$  and then increase with frequency. This does not occur for the dipoles because the SAR distributions for monopoles are different than dipoles. There are multiple SAR hot spots for the monopoles (caused by the current distribution along the metallic box) while there is a distinct one hot spot for the dipoles.



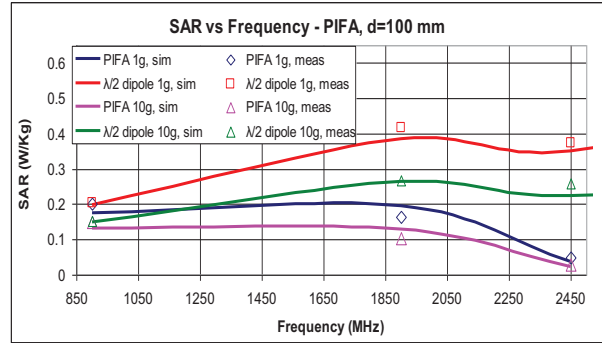
(a)



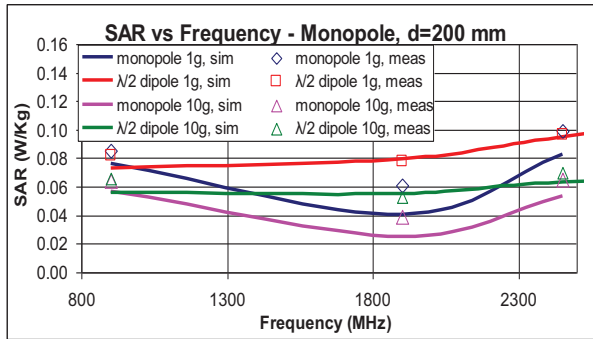
(a)



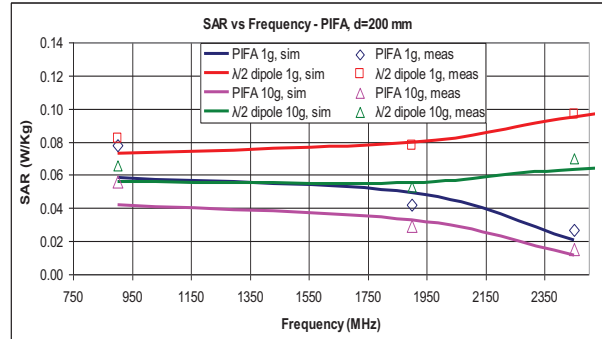
(b)



(b)



(c)



(c)

Fig. 3. SAR versus frequency of monopole antennas for  $d=40$  mm and  $d=100$  mm.

Fig. 4. SAR versus frequency of PIFAs in conventional orientation for  $d=40$  mm, 100 mm and  $d=200$  mm.

**C. SAR results of planar inverted-F antennas (PIFAs)**

SAR induced by planar inverted-F antennas (PIFAs) in the conventional orientation with respect to the phantom (here the antenna faces away from the phantom) for  $d=40$ , 100, and 200 mm are shown in Figs. 4 (a)-(c). At  $d=40$  mm, the SAR due to PIFAs decrease with frequency monotonously like that for the monopole antennas on boxes. In almost all cases the SAR due to PIFAs is smaller than the SAR due to  $\lambda/2$  dipoles except for the PIFA operating at 900 MHz and  $d=40$  mm.

Nevertheless, even in this case the SAR due to a  $\lambda/15$  dipole is considerably higher (4 W/kg – Fig. 2 (a)) than that due to the PIFA in question here (3 W/kg). For larger distances (e.g.,  $d=100$  and 200 mm), the rate of decrease in SAR from 1900 MHz to 2450 MHz is rapid. This occurs because the 2450 MHz PIFAs being printed on FR4 substrates are lossy ( $\tan\delta=0.02$ ) as opposed to the 900 and 1900 MHz PIFAs which are fabricated in air. This results in decreased SAR which did not occur for the dipoles or the quarter-wave monopoles on boxes. For example, at  $d=200$  mm and at 2450 MHz the power dissipated for a  $\lambda/2$  dipole in the tissue was

0.112W out of 1W of input power. By contrast, for the same distance and at the same frequency the power lost in the FR4 substrate was 0.504W and the power dissipated in the tissue was 0.0283W.

**D. Comparison**

SAR induced by other antenna types, sizes were also simulated and measured. All simulation and measurement data are available in [30] and [31]. However, for the sake of clarity and brevity instead of showing SAR results for each individual antenna class separately, a comparison of the simulated peak 1-g averaged SAR induced by all low directivity antennas studied are plotted as scatter plots in Fig. 5 (i). The same for peak 10-g averaged SAR induced by all low directivity antennas studied are plotted as scatter plots in Fig. 5 (ii).

For comparison, the SAR induced by single microstrip patch antennas radiating directly towards the phantom are also shown in these figures. Microstrip patch results are available at 1900, 2450, 3700, and 6000 MHz. It is evident from Figs. 5 (i) and 5 (ii) that, patches radiating away from the phantom (ground plane facing the phantom) induce very low SAR.

Comparing the peak 1-g SAR data at all three distances it is clear that:

- Except for the microstrip patch antennas that are radiating directly towards the phantom, the SAR induced by dipole antennas are the highest compared to all antennas in this study. This observation is consistent with our earlier work [25].

When comparing the SAR due to dipoles and patches flipped, it is clear that:

- At 1900 MHz, the SAR due to patches at all three distances are smaller than the SAR due to dipoles or about the same.
- At 2450 MHz, the SAR due to patches is only slightly higher than the SAR due to dipoles.
- At 3700 MHz and higher, the SAR due to patches are consistently higher than the SAR due to dipoles. Specifically at 6000 MHz and at  $d=200$  mm, the SAR due to a flipped patch is about 3 times the SAR due to a dipole.

To put these results in perspective, the near-field and radiating near-field boundaries of different antenna apertures are plotted in Fig. 6. For antennas smaller than  $0.5\lambda$ , this boundary was evaluated as  $\lambda/2\pi$ . At 900 MHz, this boundary starts at a radius of 50 mm from the antenna. As the frequency increases the radius of

this boundary decreases and vice versa. This is exactly what we see from the 1-g SAR data of the flipped patches. When the frequency is sufficiently high, e.g., 6 GHz the phantom is indeed in the far field of the antenna and thus the 1-g SAR induced is the SAR due to a small dipole (at that frequency and distance) times the linear gain of the patch antenna over the dipole.

However, if the phantom is not sufficiently in the far field, then estimating SAR by multiplying dipole SAR with the linear gain of the directive antenna will result in an over estimation of the SAR. Now for low directivity antennas that are strictly in the near field, we examine in the following if our earlier developed formulas that were reported in [25] can still be used at other distances than they were originally developed for (antenna to phantom separation,  $s < 25$  mm).

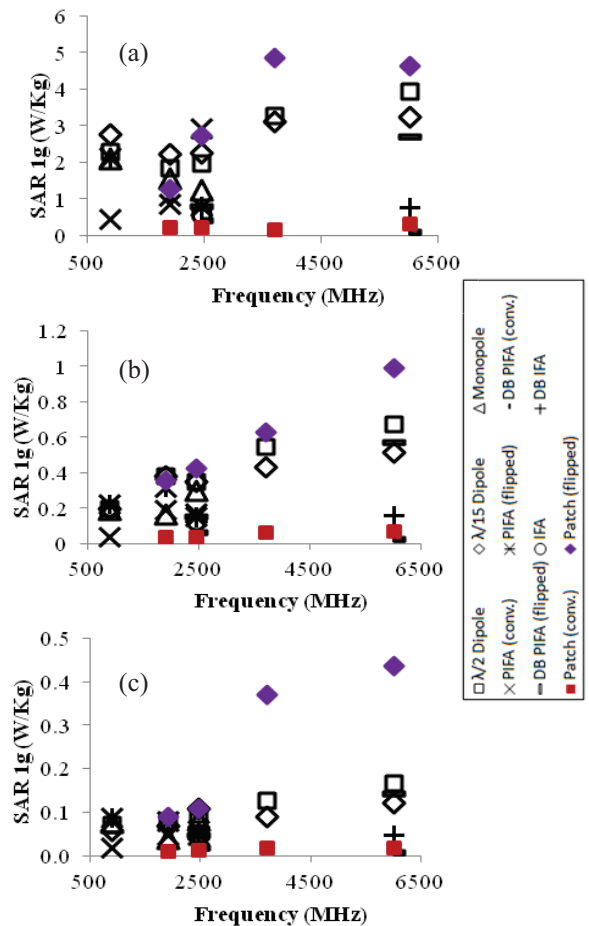


Fig. 5 (i). Peak 1-g averaged SAR comparison of all antennas at 40, 100, and 200 mm distances.

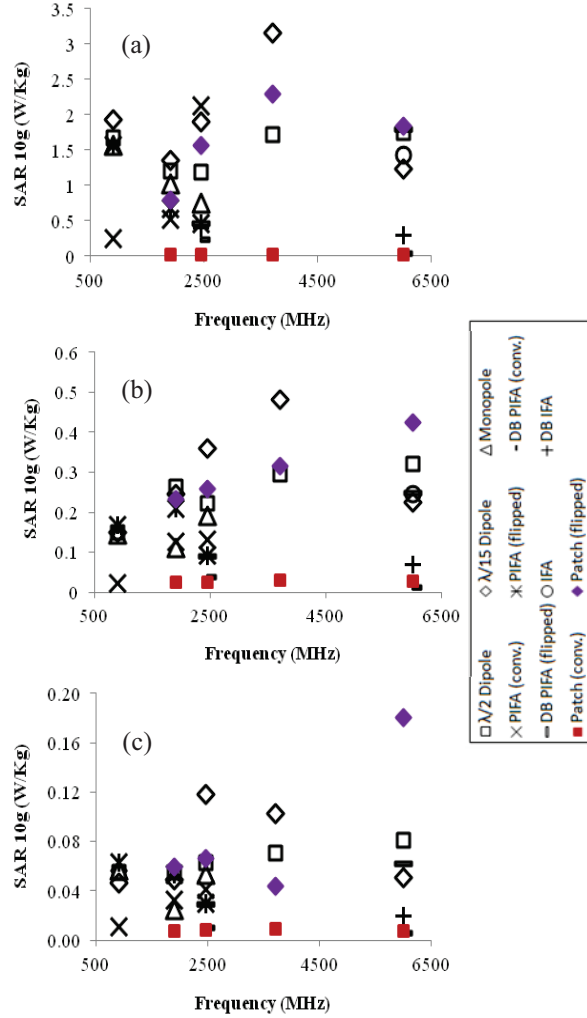


Fig. 5 (ii). Peak 10-g averaged SAR comparison of all antennas at 40, 100, and 200 mm distances.

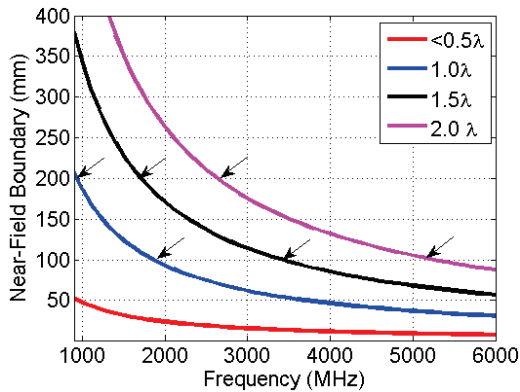


Fig. 6. Near-field boundary distances of different apertures.

In contrast, peak 10-g averaged SAR data plotted in Fig. 5 (ii) clearly shows that the only frequency at

which the SAR due to the flipped patch is higher than the dipoles is only 6 GHz. This can be explained by the fact that, under far field conditions, the patch in flipped orientation causes a more focused SAR hot spot on the phantom when compared to the dipoles. This is not the case when the phantom is in the near field of the antennas. The general trend of lower average SAR values for larger averaging volumes is therefore increasingly more enhanced for the patch antenna when the distance between patch antenna and phantom approaches or exceeds the near-field/far field boundary distance. In [25], we developed a rationale to estimate the threshold power that corresponded to the 1-g and 10-g averaged SAR based on the operating frequency,  $f$ , antenna to phantom separation,  $s$ , and the antenna half power free-space bandwidth,  $BW$ . This equation is given below:

$$P_{max,m} = \exp(As + Bs^2 + C \ln(BW) + D). \quad (1)$$

Both 1-g and 10-g averaged SAR can be calculated from (2) if  $P_{max,m}$  is known from (1) and considered as a best fit underestimate for  $P_{th,m}$ :

$$SAR_m = P_i \frac{SAR_{limit,m}}{P_{th,m}}. \quad (2)$$

This led to the following solution for  $SAR_{1g}=1.6$  W/kg:

$$A = (-0.4922f^3 + 4.831f^2 - 6.620f + 8.312)/100, \quad (3a)$$

$$B = (0.1191f^3 - 1.470f^2 + 3.656f - 1.697)/1000, \quad (3b)$$

$$C = (-0.4228f^3 + 13.24f^2 - 108.1f + 339.4)/1000, \quad (3c)$$

$$D = -0.02440f^3 + 0.4075f^2 - 2.330f + 4.730. \quad (3d)$$

For  $SAR_{10g}=2$  W/kg, the following solution was obtained:

$$A = (-0.4588f^3 + 4.407f^2 - 6.112f + 2.497)/100, \quad (4a)$$

$$B = (0.1160f^3 - 1.402f^2 + 3.504f - 0.4367)/1000, \quad (4b)$$

$$C = (-0.1333f^3 + 11.89f^2 - 110.8f + 301.4)/1000, \quad (4c)$$

$$D = -0.03540f^3 + 0.5023f^2 - 2.297f + 6.104. \quad (4d)$$

In (3) and (4),  $f$  is expressed in GHz. The free-space BW (assuming antennas are perfectly matched at their operating frequencies using lossless components) of dipole antennas are listed in Table 5.

Table 5: Dipole antenna half power free-space bandwidth. Wire radius 1.8 mm for  $f < 3.7$  GHz and wire radius=0.5 mm for  $f > 3.7$  GHz

| f (GHz)      | 0.9  | 1.9  | 2.45 | 3.7  | 6    |
|--------------|------|------|------|------|------|
| $\lambda/15$ | 0.22 | 0.32 | 0.41 | 0.50 | 0.96 |
| $\lambda/2$  | 22.2 | 28.2 | 29.6 | 45.5 | 60.2 |

The objective of equations (1)-(4) is to provide a conservative estimate of  $P_{max,m}$  or  $SAR_m$  for  $s < 25$  mm for small low directivity apertures, such as dipoles, monopoles, PIFAs IFAs etc. However, applying  $s=38$  mm (which is  $d=40$  mm in Fig. 1) in equations (1)-(4) and

using the BW data for the  $\lambda/15$  dipole in Table 5, results in 1-g SAR values of 6.44, 3.17, 2.38, 2.12, and 33.8 W/kg at 0.9, 1.9, 2.45, 3.7, and 6 GHz. Comparing these data with the actual simulated data shown in Fig. 2 (a), it is clear that the data agrees well for frequencies of up to 2.45 GHz. The corresponding estimated 10-g SAR values of 2.74, 1.26, 0.90, 0.69, and 8.8 W/kg at 0.9, 1.9, 2.45, 3.7, and 6 GHz agree reasonably well for frequencies of up to 1.9 GHz when compared with the actual simulated data shown in Fig. 2 (a).

To be conservative, if we observe the near-field boundary defined by Fig. 6 at 40 mm distance, only the SAR for  $f < 1.9$  GHz could be estimated with reasonable accuracy. Thus, the data at higher frequencies cannot be estimated using equations (1)-(4). Therefore, to apply equations (1)-(4) for  $s > 25$  mm, the frequency that corresponds to  $s = \lambda/2\pi$  should be first determined and then  $P_{max,m}$  or  $SAR_m$  should be estimated at frequencies below that.

Note that, for frequencies of 300, 400, and 500 MHz the cutoff distances are 159, 119, and 95 mm respectively. Therefore, it is plausible that at frequencies such as 300, and 400 MHz the range over which equations (1)-(4) can be used may be extended pending further numerical and experimental validation.

### E. SAR results of antenna arrays

Computed and measured peak 1-g and 10-g SAR results for the patch arrays in the flipped orientation are plotted in Figs. 7 (a)-(c). For comparison, the simulated SAR of  $\lambda/15$  dipoles are also shown. It is clear that for  $d=40$  mm the patch flipped arrays only induce higher SAR compared to a  $\lambda/15$  dipole at frequencies above 3700 MHz. For  $d=100$  MHz, this occurs at 2450 MHz, and for  $d=200$  mm at 1900 MHz.

Thus, at higher frequencies and larger distances the SAR induced by antenna arrays are substantially higher. The phenomena of lower SAR at shorter distances and lower frequencies and higher SAR at longer distances and higher frequencies will be explained in details in section V. Simulated peak 1-g and 10-g averaged SAR data of linear 3, 5, and 7 element dipole arrays at 2450 MHz and 200 mm from the phantom are shown in Table 6. For comparison, the SAR data of a single  $\lambda/2$  dipole, a single flipped patch and a 4 element patch array are also shown. Interestingly, the N=3 element array with reflector induces roughly the same SAR as the 4-element patch array. Note that, the directivities of these two arrays are very close.

Increasing the number of elements for the dipole array does not increase the SAR linearly as expected, because with increasing array size two things occur: (1) a larger array for the fixed distance means that the phantom moves more and more to the near/radiating near field, and (2) the array size becomes an

appreciable fraction of the phantom size.

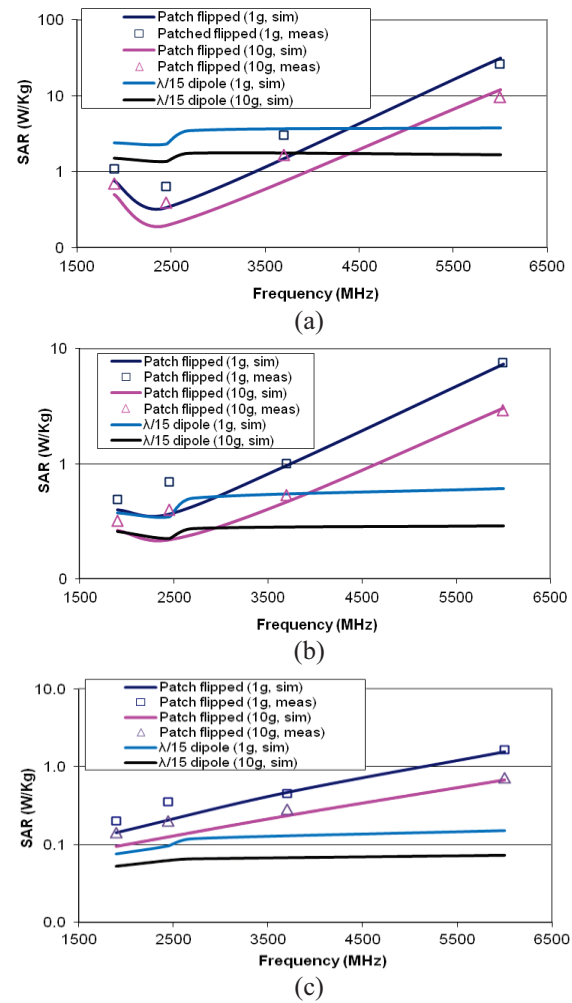


Fig. 7. SAR vs. frequency of patch antenna arrays at 40, 100, and 200 mm distance (flipped orientation).

Table 6: Comparison of SAR induced by linear dipole arrays with other antennas. Linear dipole arrays with 3, 5, 7 elements with and without reflector at 2450 MHz and 200 mm from the phantom

| Antenna Type               | $D_0$ (linear) | SAR 1g (W/Kg) | SAR 10g (W/Kg) | Dim. (mm) |
|----------------------------|----------------|---------------|----------------|-----------|
| $\lambda/2$ dipole         | 1.75           | 0.0949        | 0.0633         | 51        |
| 3 dipole array             | 4.24           | 0.1779        | 0.1087         | 196       |
| 3 dipole array & reflector | 18.3           | 0.4816        | 0.2943         | 352       |
| 5 dipole array             | 6.77           | 0.108         | 0.0573         | 335       |
| 5 dipole array & reflector | 28.18          | 0.2529        | 0.1554         | 488       |
| 7 dipole array & reflector | 38.85          | 0.1699        | 0.1045         | 627       |
| 4 patch array              | 20.89          | 0.45          | 0.28           |           |
| 1 patch                    | 2.28           | 0.1088        | 0.0677         |           |



#### IV. ANALYSES

From [8], the SAR induced in an infinite lossy plane considering plane wave analysis is given by:

$$SAR = \frac{\sigma}{\rho} \frac{\mu\omega}{\sqrt{\sigma^2 + \varepsilon^2 \omega^2}} (1 + c_{corr} \gamma_{pw})^2 H_{tinc}^2 \quad (5)$$

where  $\varepsilon$  is the tissue permittivity,  $\mu = \mu_0 = 4\pi \times 10^{-7}$  H/m is the tissue permeability,  $\sigma$  is the tissue conductivity,  $\rho$  is the tissue mass density,  $H_{tinc}$  is the rms value of the incident magnetic field intensity, and  $\gamma_{pw}$  is the plane wave reflection coefficient for the  $H_{tinc}$  field. Also note that,

$$\varepsilon' = \varepsilon - \sigma / j\omega \quad (6)$$

and

$$\gamma_{pw} = \frac{2|\sqrt{\varepsilon'}|}{\sqrt{\varepsilon'} + \sqrt{\varepsilon_0}} - 1 \quad (7)$$

where  $\varepsilon_0 = 8.854 \times 10^{-12}$  F/m is the free-space permittivity.

Considering 1 W transmit power, the power density caused by an isotropic antenna at a distance of  $r$  from the antenna is  $P_D = 1/(4\pi r^2)$ . Considering a  $\lambda/2$  dipole antenna with directivity of 1.64 the  $P_D = 1.64/(4\pi r^2)$ , which results in  $H_{tinc} = P_D / 377$ .

Considering the permittivity, conductivity, and mass density values of the homogeneous phantom given in Table 4, the above equations were used to calculate SAR as function of frequency on the surface of an infinite lossy media. After that, SAR was calculated at depths of up to 23 mm of the lossy surface at 1 mm intervals using the skin depth formula below. From these table of SAR values the 1-g and 10-g averaged SAR data were calculated:

$$\delta = \frac{1}{\omega} \left[ \left( \frac{\mu_0 \varepsilon_r \varepsilon_0}{2} \right) \left( \sqrt{1 + \left( \frac{\sigma}{\omega \varepsilon_0 \varepsilon_r} \right)^2} - 1 \right) \right]^{-1/2} \quad (8)$$

Calculated SAR data using this method are compared with direct simulation and measurement data for dipoles and monopoles at 40, 100, and 200 mm distance in Fig. 8.

For antennas smaller than half-wavelength, the near field boundary is 50 mm at 900 MHz. This agrees with the results shown in Fig. 8. As seen at 40 mm distance, the only frequency at which the plane wave approximation for both 1-g and 10-g SAR deviates is 900 MHz. Thus, SAR caused by dipoles and monopoles for frequencies below 900 MHz should be estimated using our earlier proposed free-space bandwidth based approximation method. For distances greater than 50 mm, the phantom is in the far field of the small low

directivity antennas. Thus, SAR can be estimated using the plane wave approximation.

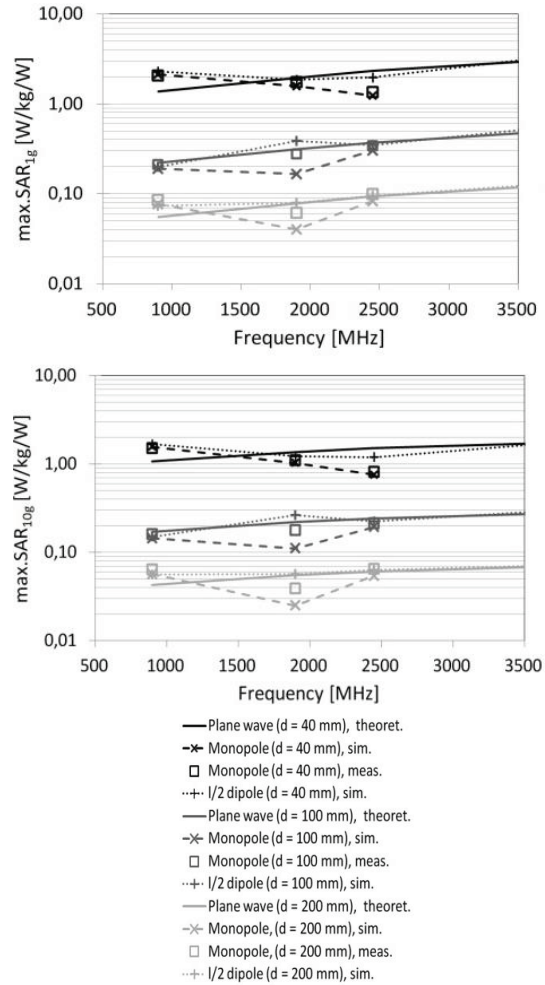


Fig. 8. Comparison of plane wave calculated SAR (dipole fed with 1 W) and SAR results obtained from direct simulations.

For large aperture directive antennas that radiate directly towards the phantom SAR estimation is not so simple. One may consider the EIRP (effective isotropically radiated power) instead of the power to estimate the SAR. Thus, if the transmit power is  $P_t$  and the antenna gain is  $G_t$ , then the EIRP should be  $P_t G_t$ . Thus, if the antenna gain is 10 times the gain of a small dipole antenna, the SAR should be multiplied by 10. However, this will only satisfy if the aperture is sufficiently far from the phantom or body such that the aperture far field radiation beam has formed. It is difficult to pin-point the exact far field distance because it will depend on the aperture electrical size and the frequency of operation. From Table 7, it is clear that for a fixed antenna to phantom separation the smaller the aperture the lower is the frequency where the near-field

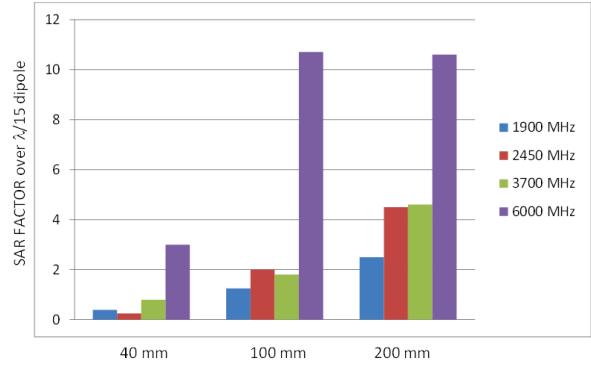
boundary transition takes place. Conversely for a fixed aperture, say  $1.5\lambda$ , if the antenna to phantom distance increases, the reactive near-field to radiating near-field boundary occurs at a lower frequency. Thus, it is clear that for a fixed aperture size and fixed antenna to phantom separation the higher the frequency the more the likelihood that the aperture far-field beam will have formed. Thus, for similar directivity apertures (meaning apertures with similar dimensions) the SAR is likely to be much higher at higher frequencies simply because the directive beam has formed.

Table 7: Aperture size and near-field boundary for directive apertures

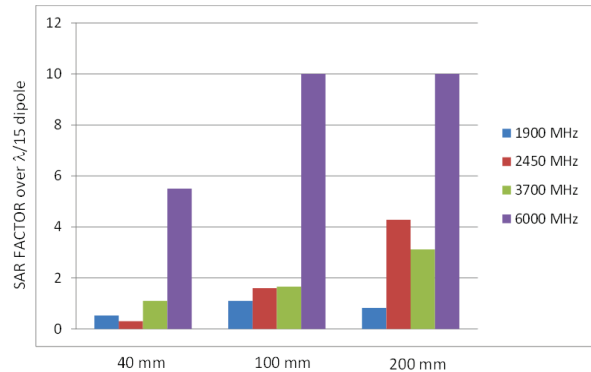
| Aperture to phantom distance | Aperture Size |              |            |
|------------------------------|---------------|--------------|------------|
|                              | $1\lambda$    | $1.5\lambda$ | $2\lambda$ |
| 100 mm                       | 1900 MHz      | 3500 MHz     | 5200 MHz   |
| 200 mm                       | 900 MHz       | 1800 MHz     | 2800 MHz   |

## V. DISCUSSIONS

Figures 9 (a) and 9 (b) illustrate the SAR factors (SF) of patch arrays over  $\lambda/15$  dipole antennas for various frequencies at various distances from the phantom. Peak 1-g average SAR factors of planar patch arrays over a  $\lambda/15$  dipole antenna show that at 40 mm distance only the 6000 MHz array has an SAR factor larger than 1. At 100 mm most patch arrays have an SAR factor  $>1$  but  $<2$  except the 6 GHz patch array which has an SAR factor  $>10$ . At 200 mm all patch arrays have an SAR factor  $>1$  and the 6 GHz patch array has an SAR factor  $>10$ . Two factors in play are array size with respect to phantom and array electrical distance from phantom. It must be noted that all results presented here are based on SAR analysis in homogeneous phantoms as used for compliance testing according to IEC 62209-2 [29]. As reported in [32] and [33], 1-g and 10-g averaged SAR results obtained in homogeneous phantoms according to [29] can underestimate the corresponding SAR in anatomical body models when the body or phantom is no longer in the reactive near field of the antenna. The reasons for this phenomenon are standing wave effects in low conductivity tissue layers which may appear in worst case tissue layer compositions. According to [32] and [33], the extent of the possible underestimation depends on frequency and distance to the antenna and lies in the range of 2.2 to 4.7 dB. In order to stay conservative, all estimated SAR values based on the results presented in the present paper should be correspondingly scaled taking into account the results reported in [32] and [33].



(a) 1-g average SF



(b) 10-g average SF

Fig. 9. SAR factors (SF) of patch arrays over  $\lambda/15$  dipole antennas.

## VI. CONCLUSIONS

The SAR induced in a large 600 mm by 400 mm by 150 mm elliptical flat phantom by a large class of small low directivity antennas and directive patch antennas and arrays at distances of 40, 100, and 200 mm are studied and analyzed. The frequency range within which the study is conducted is from 900-6000 MHz. Both simulation and measurement results are presented which illustrate a number of significant findings. It is observed that for small low directivity antennas, the SAR may be estimated using our earlier reported antenna free-space bandwidth based formulas when the phantom is still within the near field boundary of the antenna. Conversely, if the phantom is clearly in the far field, SAR can be estimated using plane wave approximation methods by multiplying with the proper linear antenna gain. For directive antennas and arrays radiating directly towards the phantom, the plane wave approximation for SAR and multiplying by the linear gain allows a good estimate as long as the phantom is clearly in the far field of the aperture. For phantoms in the near field or radiating near field, estimating the SAR using this method will result in an overestimation

due to the fact that the radiation beam has not formed yet and that the aperture could be physically larger than the phantom resulting in multiple diffused distributions. The presented results do not consider the standing wave effects in a layered tissue structure.

### ACKNOWLEDGMENT

This work was supported in part by the Mobile Manufacturers Forum (MMF), Brussels, Belgium.

### REFERENCES

- [1] Federal Communications Commission Office of Engineering and Technology Supplement C (ed. 01-01) to OET Bulletin 65 (ed. 97-01), *Evaluating Compliance With FCC Guidelines for Human Exposure to Radiofrequency Electromagnetic Fields, Additional Information for Evaluating Compliance of Mobile and Portable Devices with FCC Limits for Human Exposure to Radiofrequency Emissions*, Washington, DC, Jun. 2001.
- [2] Council of the European Union, *Council Recommendation of July 12, 1999 on the Limitation of Exposure of the General Public to Electromagnetic Fields (0 Hz - 300 GHz)*, Document 1999/519/EC, Official Journal of the European Communities, pp. L199/59-L199/70, Jul. 30, 1999.
- [3] IEEE Stand. for Safety Levels with Respect to Human Exposure to Radio Frequency Electromagnetic Fields, 3 kHz to 300 GHz, IEEE Stand. C95.1-1991.
- [4] IEEE Stand. for Safety Levels with Respect to Human Exposure to Radio Frequency Electromagnetic Fields, 3 kHz to 300 GHz, IEEE Stand. C95.1-2005.
- [5] ICNIRP, "International commission on non-ionizing radiation protection guidelines for limiting exposure to time-varying electric, magnetic and electromagnetic fields (up to 300 GHz)," *Health Physics*, vol. 74, no. 4, pp. 494-522, 1998.
- [6] Q. Balzano, O. Garay, and T. J. Manning, "Electromagnetic energy exposure of simulated users of portable cellular telephones," *IEEE Trans. Veh. Technol.*, vol. 44, no. 3, pp. 390-403, Aug. 1995.
- [7] T. Schmid, O. Egger, and N. Kuster, "Automated E-field scanning system for dosimetric assessments," *IEEE Transactions on Microwave Theory and Techniques*, vol. 44, no. 1, pp. 105-113, Jan. 1996.
- [8] N. Kuster and Q. Balzano, "Energy absorption mechanism by biological bodies in the near field of dipole antennas," *IEEE Trans. Veh. Technol.*, vol. 41, no. 1, pp. 17-23, Feb. 1992.
- [9] M. A. Jensen and Y. Rahmat-Samii, "EM interaction of handset antennas and a human in personal communications," in *Proc. IEEE*, vol. 83, no. 1, pp. 7-17, Jan. 1995.
- [10] M. Okoniewski and M. A. Stuchly, "A study of the handset antenna and human body interaction," *IEEE Trans. Microwave Theory Tech.*, vol. 44, no. 10, pp. 1855-1864, Oct. 1996.
- [11] V. Hombach, K. Meier, M. Burkhardt, E. Kühn, and N. Kuster, "The dependence of EM energy absorption upon human head modeling at 900 MHz," *IEEE Trans. Microwave Theory Tech.*, vol. 44, pp. 1865-1873, Oct. 1996.
- [12] K. Meier, V. Hombach, R. Kästle, R. Y-S. Tay, and N. Kuster, "The dependence of electromagnetic energy absorption upon human-head modeling at 1800 MHz," *IEEE Trans. Microwave Theory Tech.*, vol. 45, pp. 2058-2062, Nov. 1997.
- [13] S. Watanabe, M. Taki, T. Nojima, and O. Fujiwara, "Characteristics of the SAR distributions in a head exposed to electromagnetic fields radiated by a hand-held portable radio," *IEEE Trans. Microw. Theory Tech.*, vol. 44, no. 10, pp. 1874-1883, Oct. 1996.
- [14] O. P. Gandhi, G. Lazzi, and C. Furse, "Electromagnetic absorption in the human head and neck for mobile telephones at 835 and 1900 MHz," *IEEE Trans. Microwave Theory Tech.*, vol. 44, no. 10, pp. 1884-1897, Oct. 1996.
- [15] Q. Balzano, M. Y. Kanda, and C. C. Davis, "Specific absorption rates in a flat phantom in the near-field of dipole antennas," *IEEE Trans. Electromagn. Compat.*, vol. 48, no. 3, pp. 563-568, Aug. 2006.
- [16] C. C. Davis, B. B. Beard, A. Tillman, J. Rzasa, E. Merideth, and Q. Balzano, "International intercomparison of specific absorption rates in a flat absorbing phantom in the near-field of dipole antennas," *IEEE Trans. Electromagn. Compat.*, vol. 48, no. 3, pp. 579-588, Aug. 2006.
- [17] G. Lazzi and O. P. Gandhi, "On modeling and personal dosimetry of cellular telephone helical antennas with the FDTD code," *IEEE Trans. Antennas Propagat.*, vol. 46, pp. 525-530, Apr. 1998.
- [18] P. Bernardi, M. Cavagnaro, S. Pisa, and E. Piuze, "Power absorption and temperature elevations induced in the human head by a dual-band monopole-helix antenna phone," *IEEE Trans. Microw. Theory Tech.*, vol. 49, no. 12, pp. 2539-2546, Dec. 2001.
- [19] M. Ali, M. G. Douglas, A. Faraone, and C-K. Chou, "Upper bounds of SAR for dipole antennas

- in the 300-3000 MHz frequency range,” Proceedings of the *Bioelectromagnetics Society Conference*, Dublin, Ireland, Jun. 19-24, 2005.
- [20] A. T. M. Sayem, M. Ali, G. Schmid, and N. Haas, “Bandwidth, efficiency, and SAR of canonical antennas,” Proceedings of the *Bioelectromagnetics Society Conference*, Cancun, Mexico, Jun. 2006.
- [21] M. Ali, M. G. Douglas, A. T. M. Sayem, A. Faraone, and C-K. Chou, “Threshold power of canonical antennas for inducing SAR at compliance limits in the 300-3000 MHz frequency range,” *IEEE Transactions on Electromagnetic Compatibility*, vol. 49, pp. 143-152, Jan. 2007.
- [22] A. T. M. Sayem, G. Schmid, B. Petric, M. G. Douglas, and M. Ali, “SAR induced by monopole and planar antennas to determine threshold power levels of wireless devices,” *29<sup>th</sup> Annual Meeting of the Bioelectromagnetic Society*, Abstract book, pp. 210-214, Kanazawa, Japan, Jun. 2007.
- [23] A. T. M. Sayem, G. Schmid, N. Haas, B. Petric, M. G. Douglas, and M. Ali, “Correlating bandwidth and efficiency with SAR of monopole antennas in the 300-6000 MHz band,” *European Bioelectromagnetics Conference*, Bordeaux, France, Apr. 2007.
- [24] A. T. M. Sayem, G. Schmid, M. G. Douglas, and M. Ali, “Comparing the SAR induced by wire and planar antennas in a flat phantom,” *30<sup>th</sup> Annual Meeting of the Bioelectromagnetic Society*, Abstract book, pp. 290-292, San Diego, CA, 2008.
- [25] A. T. M. Sayem, M. Ali, G. Schmid, B. Petric, and M. G. Douglas, “Correlating threshold power with free-space bandwidth for low directivity antennas,” *IEEE Transactions on Electromagnetic Compatibility*, pp. 25-37, Feb. 2009.
- [26] IEC Stand. 62479, *Assessment of the Compliance of Low Power Electronic and Electrical Equipment with the Basic Restrictions Related to Human Exposure to Electromagnetic Fields (10 MHz - 300 GHz)*, ed. 1, Jun. 2010.
- [27] Md. A. B. Mazady, G. Schmid, R. Überbacher, M. G. Douglas, and M. Ali, “SAR induced by dipole antennas to determine low power thresholds for wireless transmitters at distances of 25-200 mm from the user,” *Bioelectromagnetics Society Conference*, Davos, Switzerland, Jun. 2009.
- [28] Md. A. B. Mazady, G. Schmid, R. Überbacher, G. Bit-Babik, and M. Ali, “SAR induced by resonant antennas at distances of 40 and 200 mm from an elliptical phantom,” *Bioelectromagnetics Society Conference*, Seoul, Korea, Jun. 2010.
- [29] IEC Stand. 62209-2, *Human Exposure to Radio Frequency Fields from Handheld and Body-Mounted wireless Communication Devices - Human Models, Instrumentation and Procedures - Part 2: Procedure to Determine the Specific Absorption Rate SAR for Wireless Communication Devices Used in Close Proximity to the Human Body (Frequency Range 30 MHz - 6 GHz)*, ed. 1, Mar. 2010.
- [30] Md. A. B. Mazady, *Electromagnetic Exposure in a Phantom in the Near and Far Fields of Wire and Planar Antennas*, M.S. Thesis, University of South Carolina, 2010.
- [31] *Quarterly Reports (Eight Reports) on Work Package 3 - Low Power Exemption Rationale for Wireless Transmitters at Distances of 25 mm or Greater from the User*, Mobile Manufacturers Forum, 2008-2010.
- [32] A. Christ, A. Klingeböck, T. Samaras, C. Goiceanu, and N. Kuster, “The dependence of electromagnetic far-field absorption on body tissue composition in the frequency range from 300 MHz to 6 GHz,” *IEEE Trans. Microwave Theory Tech.*, vol. 54, pp. 2188-2195, May 2006.
- [33] A. Christ, T. Samaras, A. Klingeböck, and N. Kuster, “Characterization of the electromagnetic near-field absorption in layered biological tissue in the frequency range 30 MHz to 6000 MHz,” *Phys. Med. Biol.*, 51, pp. 4951-4965, 2006.